NOVA SCHOOL OF SCIENCE & TECHNOLOGY

DEPARTAMENT OF MATERIALS SCIENCE

HÉLDER AZEVEDO MARINHO

BSc in Materials Science and Engineering

ELECTROSPUN MAGNETIC POROUS MEMBRANES FOR BONE TISSUE ENGINEERING

INTEGRATED MASTER IN MATERIALS ENGINEERING

NOVA University Lisbon

September, 2023

DEPARTAMENT OF MATERIALS SCIENCE

ELECTROSPUN MAGNETIC POROUS MEMBRANES FOR BONE TISSUE ENGINEERING

HÉLDER AZEVEDO MARINHO

BSc in Materials Science and Engineering

Adviser: Doctor Marta Corvo
Researcher, i3N|Cenimat, NOVA School of Science and Technology, Lisbon

Co-adviser: Professor Doctor João Paulo Borges
Full Professor, NOVA School of Science and Technology, Lisbon

Examination Committee:

Chair: Professor Doctor Maria do Carmo Lança
Assistant Professor, NOVA School of Science and Technology, Lisbon

Rapporteur: Professor Doctor Susete Fernandes
Invited Assistant Professor, NOVA School of Science and Technology, Lisbon

Adviser: Doctor Marta Corvo
Researcher, i3N|Cenimat, NOVA School of Science and Technology, Lisbon

INTEGRATED MASTER IN MATERIALS ENGINEERING

NOVA University Lisbon
September, 2023

À minha tia Isaura e ao meu avô Azevedo.

ACKNOWLEDGEMENTS

Agradeço aos meus orientadores, Doutora Marta Corvo e Professor João Paulo Borges, pelo tempo, pela ajuda e pela paciência. Sem todo o acompanhamento que tive, não conseguiria realizar este projeto nem aprender o que aprendi ao longo do mesmo.

Agradeço também ao Professor João Canejo pelas dicas de *electrospinning*, à Doutora Paula Soares pela ajuda com os ensaios de hipertermia, à Professora Daniela Gomes pelas imagens espetaculares de SEM, à Doutora Tânia Vieira por ter conseguido fazer com que todas as células sobrevivessem e à Maria Morais pelas análises de XRD. Penso que não me esqueci de mencionar ninguém, mas agradeço a todos os Professores, alunos e funcionários do Cenimat e do DCM pela companhia e pelas dicas de laboratório.

Aos meus colegas do laboratório de NMR, por toda a ajuda, pela partilha de experiências, pela partilha de conhecimento e pelo calor humano (que tanto foi preciso!).

Aos meus pais, por tudo (patrocínio do curso incluído). À minha família, pelo apoio moral, pela preocupação e por saber que tenho sempre muita gente a torcer por mim.

Por fim (mas também importante), a todos os meus amigos por me ajudaram a sobreviver à faculdade. Aos rapazes do Secundário e da play, Bruno, David, Kx e Zé, por me fazerem sempre rir, pelos clips lendários de Pau Clubes e por não esticarem muito comigo.

Aos Discípulos do Tó e aos Calemas, Kika, Rita, Rui, Tomás, Zé Pedro e Zé Eduardo, por todos os momentos passados juntos, pelos estoiros no armário, pela carne que deu 10-0 à massa, por aquela viagem empacotadíssima, pelos refs do Jardim Bar, pelo Duplex, pelo Decretus, pelos mistos da Tojeira e da Tradição e vá, até por aquele hambúrguer frio da autoestrada.

Aos Masqueicos, António, De Marco, Gil, Inês, Lourenço, Maggie, Martim, Rita, Salgueiro, Salvador e Tomás, pelos 5 anos de Materiais, nos quais partilhámos frustrações, gargalhadas, conhecimento e também muita cerveja (honorable mention aos GdM que por razões óbvias está abreviado).

À minha Madrinha Marta e ao meu Padrinho Rocha, pelo exemplo e por toda a ajuda que me deram. Às minhas Afilhadas Carolina, Catarina e Kika e ao meu Afilhado Beirão pela confiança e por todos as dores de cabeça (no final, orgulho-me em dizer que valeram a pena!).

Às minhas Velhas, Mafalada, Peixoto e Meri, pelo apoio, pela orientação, pela amizade, pela maravilhosa *team* (em itálico, claro) agenda e pelos temidos likes nos comentários (ou nas mensagens?). Aos meus Colegas Novos, Afonso, Val, Damas, Danny, Dinis, Minnie, Johnny

Ricky, Pedro e Teresa por me darem um ano de Finalista fantástico. Pelos desabafos, pela companhia no sofrimento e na alegria, na ordem e no caos, na anarquia e na hierarquia. Pelos jantares na Redentora, pelas dormidas, pelas pós-internas e por serem o melhor *sticker material* que já vi e as melhores maçãs de sempre. Obrigado, do fundo do coração, por tudo o que esta aventura significou para mim! Se continuasse, ia passar o limite de palavras, portanto acabo com aquela intro básica: "a gente é 5, mas quando reúne, planeia bem a atividade", se bem que acho que agora já somos mesmo 7.

Obrigado a todos!

“No matter what, you keep finding something to fight for." (Joel Miller, fictional character).

ABSTRACT

Organ transplantation has been and still is the classic method to heal patients with any kind of organ disease. However, this approach has several downsides, such as donor scarcity, short preservation time of the organs, high cost, and post-operation complications. Tissue engineering, a domain that aims to develop adequate substitutes that restore, maintain, and improve tissue functions, is a relatively new alternative in the regenerative medicine field that overcomes organ transplantation issues.

In this work, new membranes for bone tissue engineering were produced from electrospun PLA membranes with poly(ionic liquid) and superparamagnetic iron oxide nanoparticles (SPIONs). The membranes were submitted to supercritical drying with CO_2, to induce porosity for better cell attachment, a procedure that also enhanced the crystallinity of the membranes. The samples were characterized by ATR-FTIR, TGA, XRD, SEM and magnetic hyperthermia. The results showed that all the samples with nanoparticles are suited for local cancer treatment, as it is possible to reach the temperature to eliminate tumoral cells by magnetic hyperthermia treatment. The samples were evaluated for cytotoxicity according to ISO 10993-5 with a human osteosarcoma cell line and the lowest registered value for cell viability was 94%, meaning that no sample presented cytotoxicity.

Keywords: bone tissue engineering, membranes, fibres, SPIONs, porosity.

RESUMO

A transplantação de órgãos tem sido e permanece como o método clássico de tratar pacientes com qualquer tipo de doença nos seus órgãos. No entanto, esta abordagem apresenta várias desvantagens, tais como escassez de dadores, curto tempo de preservação dos órgãos, custo elevado e complicações pós-operatórias. A área de engenharia de tecidos, cujo objetivo consiste no desenvolvimento de substitutos adequados que restauram, mantêm e melhoram a função dos tecidos, é uma alternativa relativamente recente no ramo da medicina regenerativa que supera os problemas da transplantação de órgãos.

Neste trabalho, novas membranas para engenharia de tecidos ósseos foram produzidas a partir de membranas eletrofiadas de PLA com um poli(líquido iónico) e nanopartículas superparamagnéticas de óxido de ferro (SPIONs). As membranas foram submetidas a secagem supercrítica com CO_2, com o objetivo de induzir porosidade, de forma a melhorar a adesão celular. Este procedimento também aumentou a cristalinidade das membranas. As amostras foram caracterizadas por ATR-FTIR, TGA, XRD, SEM e hipertermia magnética. Os resultados demonstram que todas as amostras com nanopartículas são adequadas para tratamento de cancro localizado, visto que é possível alcançar uma temperatura que elimina as células tumorais por tratamento de hipertermia magnética. As amostras foram também testadas em relação à citotoxicidade de acordo com a norma ISO 10993-5 com uma linha celular de osteossarcoma humano e o valor de viabilidade celular mais baixo obtido foi de 94%, o que significa que nenhuma amostra apresenta citotoxicidade.

Palavras-chave: engenharia de tecidos ósseos, membranas, fibras, SPIONs, porosidade.

CONTENTS

List of Figures

List of Tables

ABBREVIATIONS

AEtMAC	[2-(Acryloyloxy)-ethyl] trimethylammonium chloride
AIBA	2,2′-Azobis(2-methyl-propionamidine) dihydrochloride
ATR-FTIR	Attenuated total reflectance - Fourier transformed infrared spectroscopy
BTE	Bone tissue engineering
DCM	Dichloromethane
DMF	*N, N*-Dimethylformamide
DMSO	Dimethyl sulfoxide
ECM	Extracellular matrix
GF	Growth factor
HAp	Hydroxyapatite
IL	Ionic liquid
mNP	Magnetic nanoparticle
MRI	Magnetic resonance imaging
NMR	Nuclear magnetic resonance
NP	Nanoparticle
PCL	Polycaprolactone
PGA	Polyglycolic acid
PIL	Poly([2-(acryloyloxy)-ethyl] trimethylammonium chloride)
PLA	Polylactic acid
PLGA	Poly(lactic-co-glycolic acid)
Saos-2	Human osteosarcoma cell line
SAR	Specific absorption rate
$scCO_2$	Supercritical CO_2

SCs	Stereocomplexes
SEM	Scanning electron microscopy
SPION	Superparamagnetic iron oxide nanoparticle
TCP	Tricalcium phosphate
TGA	Thermogravimetric analysis
U.S. FDA	United Stated Food & Drug Administration
wt	weight
XRD	X-ray diffraction

1 INTRODUCTION

1.1 Tissue engineering

Tissue engineering is a multidisciplinary domain that combines engineering, materials science, and biology principles to develop adequate substitutes that restore, maintain, and improve tissue functions [1]. The term "tissue engineering" dates from the mid-80s, and it emerged from the need to upgrade organ transplantation, a method that entails some issues, such as donor scarcity, short preservation time of the organs, high overall cost, and post-operation complications [2]. One could say it all started with the transplantation of important functional cells, known as selective transplantation [3], that was later coupled to artificial biodegradable matrixes into what is known as scaffolds. These scaffolds must present specific properties: cell diffusion, proliferation and function and promotion of vascular ingrowth.

1.2 Bone

Bone is a mineralized tissue comprised mainly of hydroxyapatite (HAp) and type I collagen, while also containing water, ions, and proteins [4]. It has essential functions in the body, such as mechanical support, protection of soft tissues, locomotion, storage of calcium and phosphate, and bone marrow harbouring. Bone has four types of cells: osteoblasts, osteoclasts, osteocytes, and bone lining cells. Osteoblasts are responsible for bone tissue formation and osteoclasts for its resorption. Bone formation and resorption must be balanced, otherwise, several bone diseases will appear. Osteocytes, formed from osteoclasts, have an interconnected network that allows detection of mechanical loads by the piezoelectric effect, acting as bone remodelers through the regulation of bone formation and resorption [5]. Another important bone component is the bone extracellular matrix (ECM), made of collagen fibrils, which provide mechanical support and are crucial for bone homeostasis and for the regulation of bone cell activity [4].

Bone has an intrinsic healing capacity due to differentiation of stem cells stemming from bone marrow. Nevertheless, large bone defects, that can be caused by accidents, old age, or disease, cannot be repaired naturally, and need external intervention. The most common

method is autologous bone grafting, which involves the transport of bone from one location to the damaged site in the same patient. Even so, it brings numerous drawbacks, like high donor site morbidity and scarcity of autologous bone, which limits its application. To overcome these obstacles, bone tissue engineering (BTE) can be the solution. Its main purpose is to create functional, living bone tissue that can be integrated *in vivo* and degrade to repair damaged or diseased bone, using a combination of cells, biomaterials, growth factors (GFs) and other bioactive molecules [4].

1.3 Bone tissue engineering: scaffolds and biomaterials

Scaffolds and their fabrication have a significant role in BTE, as their goal is to mimic the ECM. An optimal scaffold should be biodegradable, bioactive, biocompatible, and non-cytotoxic while inducing the least immune response possible. Moreover, it should be receptive to the inclusion of cells, promoting their attachment, proliferation and differentiation, GFs and other bioactive molecules, and in some cases to functional nanoparticles (NPs) and medicines, that can stimulate bone regeneration [4], [6]. Figure 1 shows a schematic of a scaffold for BTE and its components.

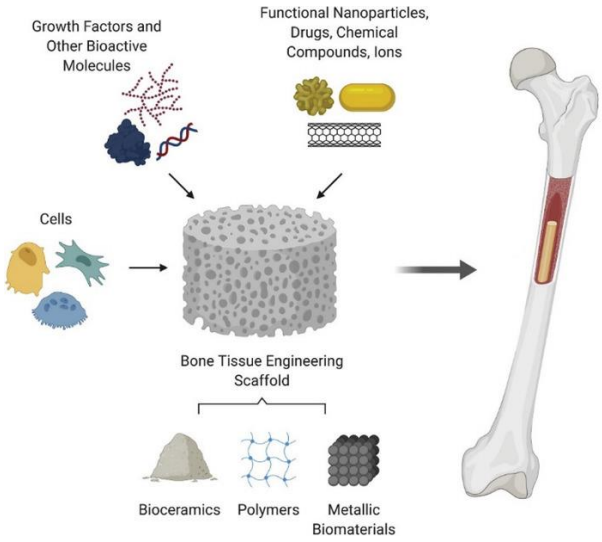

Figure 1 - Schematic of a BTE scaffold with the classes of materials used and its components, which include cells, GFs and other bioactive molecules, NPs, drugs, chemical compounds, and ions. Adapted from [6].

A large variety of biomaterials has been looked into regarding scaffolds, mainly inorganic ones, which comprehend metals (e.g., titanium alloys), bioceramics (e.g., HAp, and α, β-Tricalcium phosphates (α, β-TCP)), natural polymers (e.g., collagen, gelatin, and chitosan) and synthetic ones (e.g., polycaprolactone (PCL), polyglycolic acid (PGA), and polylactic acid (PLA)). Bioceramics present excellent biocompatibility, osteoconductivity and bioresorbability, while

polymers have high mechanical strength and stiffness. Natural polymers present the advantages of biocompatibility, resemblance to the ECM, and degradation into natural products [6]. The general materials used in scaffolds for BTE and their main respective characteristics, advantages and disadvantages are synthesised in Table A1 in the Appendix.

To improve the properties of the scaffold, mainly its processability, mechanical properties and bioactivity, one can resort to composite materials. Some examples include polymeric matrix composites reinforced with natural components, such as collagen, and ceramic matrix composites reinforced with natural or synthetic polymers [4].

Ionic liquids (ILs), which can be defined as "low melting salts" [7] can be used as a reinforcement of synthetic polymers due to their promising properties for tissue engineering applications. In particular, cholinium-based ILs present excellent biodegradability, biocompatibility, and low toxicity, while also presenting electric and piezoelectric behaviour [8].

The properties of the scaffold are influenced not only by the composing materials, but also by the whole fabrication process. Collins et al. [6] reported several methods to produce scaffolds for BTE: electrospinning, freeze drying, additive manufacturing, phase separation, gas foaming and particulate leaching.

1.4 Electrospinning

Electrospinning is a technique used to produce nanofibres with a non-woven texture, high and controlled porosity, and a high surface area/volume ratio. To perform electrospinning, a syringe is loaded with the polymeric solution, which is placed in a pump that controls the flow of the jet. The potential difference, created by the connection of the needle and the collector to opposite terminals that generates an electric field between them, leads to the ejection of the solution, which occurs when the repulsive electrostatic force surpasses the surface tension of the liquid, and to its deposition on the collector [9]. When the solution jet moves to the collector, the solvent evaporates. Ideally, the deposited material has no solvent.

The fibre formation, structure and diameter are dependent on several factors, related to the solution (polymer concentration, solvent volatility, and solution conductivity), to the process (flow rate, needle-collector distance, and applied voltage) and to the environment (temperature, and relative humidity). All these parameters must be optimized to produce fibres that can mimic the ECM structure. The polymer concentration affects the solution viscosity. Dilute solutions produce mechanically weaker fibres and solutions with a higher concentration

than a critical value do not produce fibres. According to Nemati et al. [10], the increase of the polymer concentration, while not exceeding the critical value, leads to an increase in the fibre diameter.

Some considerations about new electrospinning methodologies and the type of polymers that can be electrospun and applied to tissue engineering are issued in Section A.1 Literature revision of the Appendix.

1.5 Nanoparticles in bone tissue engineering scaffolds

The inclusion of NPs in BTE scaffolds can actively improve their properties. However, this subject needs a more comprehensive study, as several factors will influence the NP's effects in *in vivo* applications, mainly their size and stimulation of the inflammatory response. Small NPs could potentially enter the blood circulation and reach vital organs, causing serious diseases. Polymeric NPs could degrade inside the body and generate an inflammatory reaction and consequently be released by the body, losing all their therapeutic effects [11].

Magnetic nanoparticles (mNPs) can also have a positive impact on BTE. As reported by Soares et al. [9], mNPs generate heat when an alternating magnetic field is applied. Materials with superparamagnetic properties, like ferromagnetic NPs, exhibit a random flip on the direction of magnetization influenced by the temperature. Superparamagnetic iron oxide (Fe_3O_4) nanoparticles (SPIONs) are suitable for the diagnosis and treatment of cancer, also referred to as cancer theranostics. SPIONs are good contrast agents for magnetic resonance imaging (MRI) in the detection of tumoral cells. Additionally, due to the absorption power of the SPIONs, it is possible to reach temperatures above 42ºC that will eliminate tumoral cells by magnetic hyperthermia treatment.

The incorporation of SPIONs in scaffolds prepared by laser sintering of composite powders, as detailed by Shuai et al. [12], stimulates cell adhesion, proliferation, and differentiation *in vitro*. *In vivo* experiments in white rabbits were also conducted and it was registered that the presence of SPIONs accelerated bone regeneration, by contributing to improving cell activity. In this study, SPIONs created a magnetic micro-environment, in which each particle generated a nanomagnetic field, contributing to cell adhesion, proliferation, and differentiation.

1.6 Fabrication of porous nanofibres

The control over the structure of a scaffold plays a huge role in its overall performance. The technique chosen to produce a fibrous membrane and its parameters will influence pore size, shape, orientation, and interconnectivity, which will impact its behaviour when implanted. Collins et al. [6] described several studies that showed the benefits of hierarchically porous structures for BTE, as the inclusion of these types of structures improved not only the mechanical properties of the scaffolds, but also increased the degradation rate, bone formation rate and remodelling activities.

Several methods can be used to produce porous nanofibres, and most of them consist in a multiple-step process that includes a posterior drying process to induce porosity. Drying processes are usually divided into three methods: atmospheric, freeze and supercritical drying [13]. These methods and the type of gels they originate are schematized in Figure A1 in the Appendix.

Atmospheric drying is a classical drying procedure that occurs at room temperature and ambient pressure but does not ensure the preservation of the gel structure due to the surface tension of the liquid on the pores [13]. Freeze and supercritical drying are two post-treatments that originate highly porous gels [14]: freeze drying originates cryogels and supercritical drying, aerogels. Aerogels present promising characteristics, similar to the ECM, to be used as scaffolds in BTE: high porosity, low density, and high surface area [15].

Freeze drying consists of the extraction, in a high vacuum system, of the solvent by sublimation and desorption, obtaining scaffolds with an average porosity of 90% and pore size between 20 and 200 μm. Pore size is controlled by several process parameters, including freeze rate, polymer concentration and processing temperature [6].

Supercritical drying requires a fluid with a reachable critical point that allows to interchange its physical state by changing the system's temperature and pressure. If this fluid is CO_2, the membranes are submersed in ethanol in a closed chamber and gaseous CO_2 is injected. By increasing the temperature and pressure above the CO_2 supercritical point (CO_2 reaches its supercritical point at a temperature of 31.1 ºC and a pressure of 73.9 bar [16]), the CO_2 and the ethanol blend and when they are both removed from the chamber, the characteristic porosity of aerogels is induced.

Due to their hierarchically porous structure, high surface area, and good biocompatibility, aerogels are a promising material for drug loading and delivery. It is possible to deliver a fast

and local administration, as the scaffolds are implanted in the injury location, increasing, even more, bone tissue regeneration [14], [17].

1.7 Approach

Despite all the challenges and limitations yet to overcome, by combining the principles of engineering, materials science, and biology, BTE has the potential to revolutionize the way bone injuries and diseases are treated. Significant progress has been made in recent years, and it is expected that BTE will play a significant role in the future of regenerative medicine and in the well-being of mankind.

This project's objective was the production of porous membranes for BTE applications, through the electrospinning of PLA solutions, and the evaluation of the incorporation of a poly(IL) and SPIONs, and the drying treatment to induce fibre porosity.

This document is segmented into various sections. Section 2 provides an in-depth overview of the materials and methods used in this project. Section 3 elaborates on the results obtained, including their discussion and comparison to existing literature. Section 4 outlines conclusions and future perspectives, and the Appendix contains supplementary information to all sections.

2
MATERIALS AND METHODS

A detailed description of the materials and the characterization techniques used in this work can be found in more detail in Sections A.2 Materials and A.3 Characterization of the Appendix.

2.1 SPIONs synthesis

SPIONs were synthesized according to a previously described procedure [18]. Briefly, 2.5 mmol (0.50 g) of $FeCl_2 \cdot 4H_2O$ and 5 mmol (1.35 g) of $FeCl_3 \cdot 6H_2O$ were weighed and transferred to a three-neck round bottom flask of 250 mL. Then, 100 mL of ultrapure water was added, and the iron salts were dissolved under mechanical stirring at 500 rpm. The previous solution was deaerated by bubbling N_2. After closing the system, 10 mL of an aqueous ammonium solution 25% were rapidly added, and the solution changed its colour to black. After 5 minutes, the solution was transferred to a Falcon tube. To avoid leaving any NPs in the flask, 50 mL of ultrapure water were added to the flask and transferred to the same Falcon tube. The excess of solvent was removed with a pipette, and the aid of a magnet.

Oleic acid 16% (w/w) was added to the NP suspension using a micropipette with a cut tip and the solution was placed in an ultrasonic bath for 3 hours. The bath was monitored to prevent the water from heating. The NPs were then washed twice with acetone and twice with dichloromethane (DCM). The excess of the final solvent was removed to obtain a suspension of 25 mL. The NPs were aggregated, so they were subjected to sonication for a short period. The iron concentration was measured by evaporating the solvent of 1 mL of the suspension.

2.2 Poly(IL) synthesis

Poly([2-(Acryloyloxy)-ethyl] trimethylammonium chloride) (poly(AEtMAC)) was synthesized according to a previously described procedure [19]. Briefly, 2.58 mmol (0.63 g) of AEtMAC solution and 1.84×10^{-2} mmol (5×10^{-3} g) of 2,2′-azobis(2-methyl-propionamidine) dihydrochloride (AIBA) (1% wt of the monomer) were weighed and transferred to a 25 mL round bottom flask. Then, 5 g of ultrapure water (10% wt) were added, and the mixture was

bubbled with dry N_2 for 20 minutes. Afterwards, the solution was heated to 70ºC in an oil bath for 24 hours under magnetic stirring. The resulting mixture was evaporated under vacuum. A highly viscous yellow oil was obtained in a quantitative yield. Poly(AEtMAC) was characterized by attenuated total reflectance - Fourier transformed infrared (ATR-FTIR) spectroscopy, nuclear magnetic resonance (NMR) spectroscopy, and thermogravimetric analysis (TGA).

2.3 Solutions for electrospinning

Solutions for electrospinning were prepared, after optimization of the parameters based on previous works from the research group, using PLA in a solvent mixture of DCM and N,N-dimethylformamide (DMF) (17:3 v/v) with a polymer concentration of 10% wt. Subsequently, poly(AEtMAC) (5% wt) and SPIONs (8 and 12 % wt) were added according to the respective solution composition to prepare 5 different solutions, which are summarized in Table A2 in the Appendix. The solution with PLA was kept under magnetic stirring for 4 hours, only adding the DMF in the last 10 minutes. The solution with PLA and poly(AEtMAC) was kept under magnetic stirring for 5 days and, due to an incomplete dissolution of the poly(AEtMAC), 40 µL of water were added. For the preparation of the solutions with SPIONs, PLA and poly(AEtMAC) were dissolved in the solvent mixture in the conditions previously mentioned, and the SPIONs were added later. The solution was kept under mechanical stirring for 2 more hours to obtain a homogeneous solution with the SPIONs. To simplify, the nomenclature of poly(AEtMAC) and of SPIONs in the solutions was replaced by PIL and NP, respectively.

Electrospinning was performed in a homemade setup (Figure A2 in the Appendix [20]) comprising a high-voltage source, a programmable syringe pump and a metallic sheet collector covered with aluminium. The needle-collector distance was maintained constant at 15 cm. The voltage varied between 20 and 22 kV and the flow rate varied between 0.3 and 0.5 mL/h. The temperature and relative humidity were kept below 23 ºC and 50%, respectively. All the membranes were produced with a 1 mL syringe and a 25G needle. Table A3 in the Appendix summarizes the electrospinning parameters for all the produced membranes.

2.4 Supercritical drying

After electrospinning, the membranes were left to dry at room temperature. The membranes were then removed from the aluminium and prepared for supercritical CO_2 ($scCO_2$) drying. The whole process is described in Section A.5 Supercritical drying of the Appendix.

3 RESULTS AND DISCUSSION

Porous nanofibre membranes were produced via electrospinning of a PLA solution in DCM:DMF incorporated with a poly(IL) and SPIONs in order to increase the number of possible applications and enhance its functionality, followed by the drying treatment. A schematic outline is shown in Figure 2.

PLA, obtained from lactic acid, was the chosen polymer for this work because it is a promising synthetic biopolymer when it comes to biomedical applications, due to its biocompatibility, biodegradability, mechanical strength, processing capacity, non-toxicity, and low cost [21]. Moreover, it is an efficient matrix material for the controlled release of drugs in the desired locations [9].

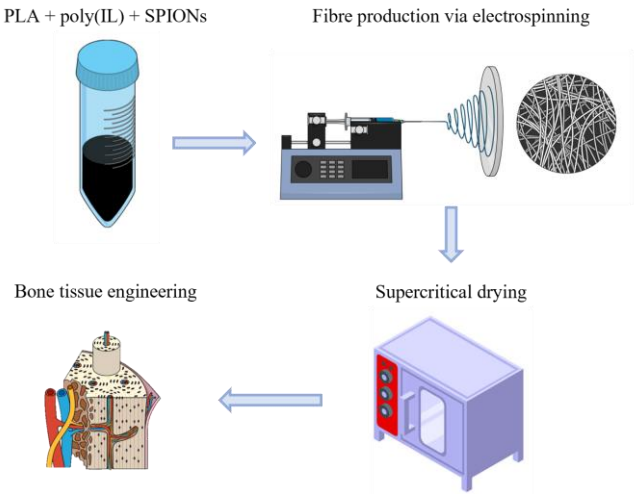

Figure 2 - Schematic outline of the present work.

In the next sections, the properties of the produced membranes will be analysed, discussed, and compared with the ones stated in the literature.

3.1 Membranes

After optimizing the electrospinning parameters in order to obtain stable and homogeneous fibres, membranes were obtained from PLA, PLA/PIL, PLA/SPIONs and PLA/PIL/SPIONs. All the obtained electrospun membranes, observed in Figure 3 still in the

aluminium foil, presented a similar appearance macroscopically, except for the colour: white in the membranes with PLA and poly(AEtMAC), and brown in the membranes with SPIONs.

Sections of the membranes were submitted to $scCO_2$ drying and both membrane types were studied via X-ray diffraction (XRD), scanning electron microscopy (SEM), magnetic hyperthermia, and cytotoxicity. ATR-FTIR and TGA were only performed in the raw membranes because the chemical structure of the samples is not expected to change with supercritical drying [14].

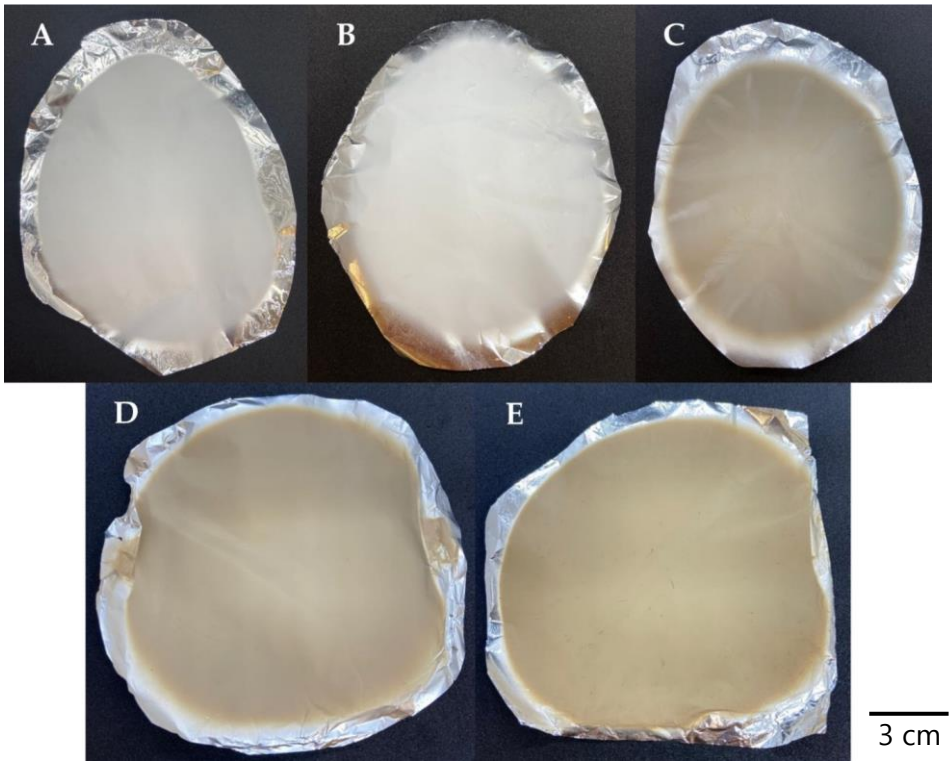

Figure 3 - Photographs of electrospun membranes: A) PLA; B) PLA/PIL5; C) PLA/NP8; D) PLA/PIL5/NP8; E) PLA/PIL5/NP12.

3.2 ATR-FTIR

Figure 4 shows the ATR-FTIR spectra of all the produced membranes. PLA shows several characteristic bands that are marked below. Bands between 2994 and 2851 cm^{-1} are relative to $-CH_3$ bonds, more specifically, at 2994 cm^{-1} is the asymmetric stretching vibration, and at 2944 cm^{-1} the symmetric stretching frequency [22]. The band observed at 1754 cm^{-1} is relative to the stretching frequency of the carbonyl group (C=O) [22]. At 1454 and 1360 cm^{-1}, the asymmetric and symmetric, respectively, bending vibration frequencies of $-CH_3$ bonds have been identified [22]. The vibration at 1184 cm^{-1} is relative to the stretching frequency of -C-O-C [23], and at

1089 cm^{-1} is due to the stretching frequency of the -C-O bond [22]. The bands observed at the lower wavenumbers, at 869 cm^{-1} and 756 cm^{-1}, represent the amorphous and crystalline phases of PLA, respectively [24].

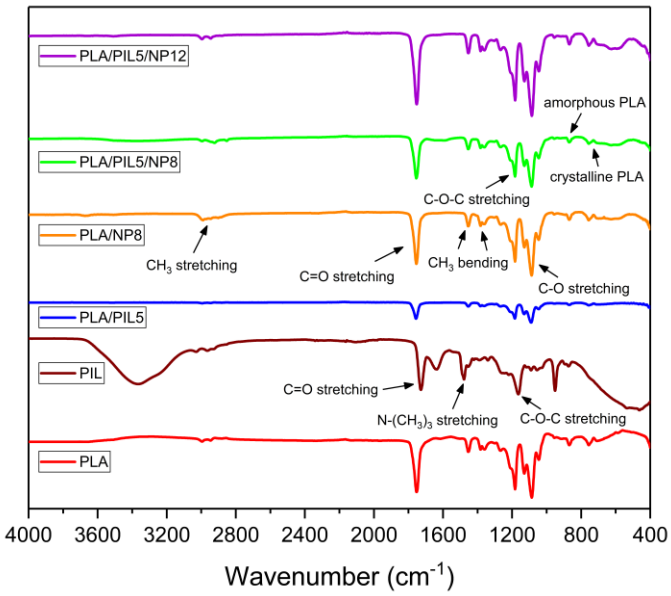

Figure 4 - ATR-FTIR spectra of PLA (red), PIL (brown), PLA/PIL5 (blue), PLA/NP8 (orange), PLA/PIL5/NP8 (green) and PLA/PIL5/NP12 (purple).

Poly(AEtMAC), referred to as PIL in Figure 4, also presents characteristic vibrations. The band at 1730 cm^{-1} is relative to the stretching vibration frequency of -C=O bond, and the band at around 1160 cm^{-1} to the stretching frequency of -C-O-C bond [25]. The band at 1500 cm^{-1} is relative to the -N-$(CH_3)_3$ bond stretching vibration.

The spectra of different membranes do not present any significant differences, which means that no new bonds or strong chemical interaction were formed when all the compounds were mixed.

3.3 Nuclear magnetic resonance

Poly(AEtMAC) obtained in quantitative yield was analysed by NMR and the obtained proton spectrum is shown in Figure 5. It is possible to verify that the polymerization was successful due to the broad peaks (larger than the monomer ones) and by the absence of the double bond signals, that would appear at lower field. It is also clear that the backbone signals, at higher field, are broader and less intense, due to the low mobility of that part of the polymeric chain. The rest of the chain has higher mobility, translating in more narrow signals. The -CH_3 connected to nitrogen atom presents the most intense signal, and the -CH_2 (c and

d), being deshielded because they are connected to an heteroatom (oxygen and nitrogen, respectively), appear at lower field. The HDO peak is related to the presence of the solvent.

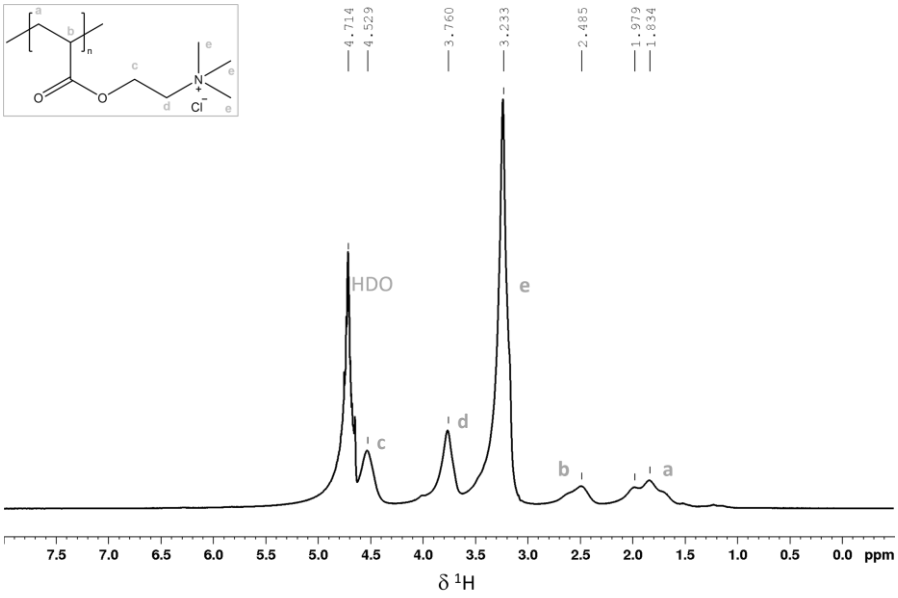

Figure 5 - NMR proton spectrum of poly(AEtMAC) and respective chemical structure.

3.4 Thermogravimetric analysis

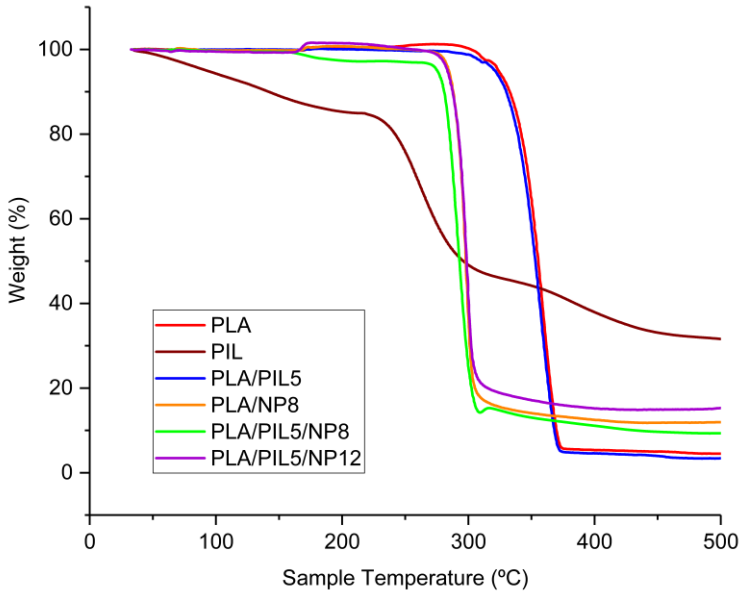

Figure 6 - TGA curves of PLA (red), PIL (brown), PLA/PIL5 (blue), PLA/NP8 (orange), PLA/PIL5/NP8 (green) and PLA/PIL5/NP12 (purple).

TGA was performed in all membranes and in poly(AEtMAC) to evaluate their thermal stability. The first significant weight loss in the membranes is detected at around 300 ºC, meaning that the membranes are chemically stable until 300 ºC. The obtained TGA curves are

shown in Figure 6. The curve of poly(AEtMAC), referred to as PIL in Figure 6, can be divided into three parts, separated by the inflection points, meaning that it has a three-step degradation profile. It starts to lose weight at a low temperature, and it could be related to the degradation of pendant groups on the polymer backbone [19]. However, the initial weight loss could also be related to water loss. Thus, one could say that the first substantial weight loss of poly(AEtMAC) starts in the first inflection point, at around 230 ºC.

As the sterilization of the samples for the cytotoxicity assays is performed at 120 ºC, it is possible to conclude that no studied material is affected by the sterilization at 120 ºC. The presence of PIL in the membranes (PLA/PIL5; PLA/PIL5/NP8 and PLA/PIL5/NP12) is not noticeable in the respective degradation profiles, most likely due to the reduced amount of PIL introduced in these samples.

The presence of SPIONs is reflected in the higher weight percentage of sample left undegraded at 500ºC, which is more noticeable for a higher amount of SPIONs.

3.5 Supercritical drying

Supercritical drying is a controlled methodology used to remove the solvent of a substance to form an aerogel. It resorts to a fluid in its supercritical phase, which brings several advantages compared to other drying processes such as ambient or freeze drying. Supercritical drying conserves the porous structure and avoids its collapsing because it does not fall back on fluids in its solid, liquid, or gaseous phase that would originate capillary forces on the pores, leading to its destruction [14]. Furthermore, the crystallization in freeze drying can lead to a volume increase that could possibly shatter the whole gel [13] and freeze drying may produce fibres with higher macroporosity than supercritical drying [14]. Supercritical drying is also able to remove any residual toxic solvents from the aerogel, making it an appealing process for biomedical applications [26], [27].

The first purpose of supercritical drying was to expand the two-dimensional electrospun membranes into three-dimensional scaffolds. However, after observation of the membranes in SEM, no expansion was registered. Other attempts were performed via depressurization of $scCO_2$, by simply placing dry ice with the membranes in a closed vessel, as reported by Li et al. [28], but the membranes remained unchanged. After careful deliberation on the next step to move forward with the project, the expansion of the membranes was abandoned. As the electrospun membranes were very thin, the expansion to up to 8 times the initial thickness [28] would probably originate scaffolds with low mechanical stability and it wouldn't be possible to

handle them. Instead, the enhancement of porosity via supercritical drying was pursued. A common drawback regarding the use of PLA in tissue engineering is its poor cell attachment. A simple solution to this problem is porosity, as many studies report an increase in cell attachment in porous nanofibres of biodegradable polymers [29].

To simplify the denominations, the samples that were not dried are from this point forward called membranes and the samples that were dried, are scaffolds, despite its definition of a "three-dimensional biomaterial that provides a suitable environment for cells to regenerate tissue and organs" [30].

3.6 X-ray diffraction

The XRD diffractograms were analysed to compare the crystallinity difference between membranes and scaffolds. As seen in Figure 7, the scaffolds present spectra with less noise, with higher intensity and thinner peaks than the membranes, which means that supercritical drying treatment increased crystallinity of the samples, as it removes any of leftover solvent, which constitutes an amorphous part of the sample. This conclusion was also reported in previous works [31]–[33]. In Figure A4 in the Appendix, it is possible to observe the spectra of all samples to compare the crystallinity difference between membranes and scaffolds.

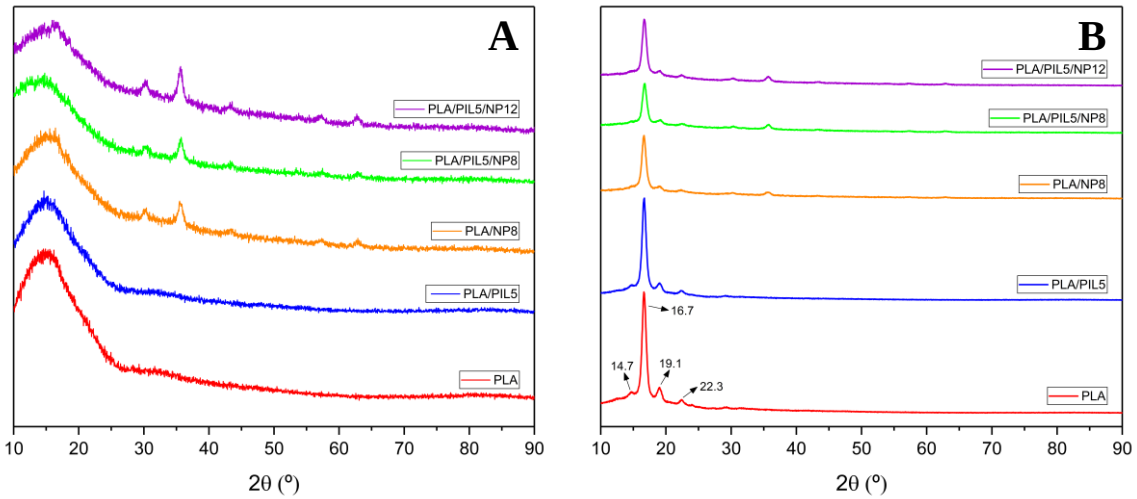

Figure 7 - XRD diffractograms of the membranes (A) and the scaffolds (B).

PLA shows its specific peaks at 2θ values of 14.7°, 16.7°, 19.1°, and 22.3°, which correspond to the peaks mentioned in the literature [34]. Also, in the samples with SPIONs, it is possible to observe the characteristic peaks of the SPIONs, which are for 2θ values of 30.6°, 36.0°, 43.6°, 57.5°, and 63.0° [35].

In general, ILs present promising properties for biomedical applications: biodegradability, biocompatibility, and low toxicity [8]. The addition of cholinium-based ILs to PLA can lead to the formation of stereocomplexes (SCs), resulting in an increase in mechanical properties. The SCs formation also means that ILs could potentially be used as a crosslinker in PLA membranes [36]. Moreover, these ILs also present piezoelectric properties due to their ionic conductivity, which can be useful in bone tissue engineering applications, as osteocytes work as bone remodelers through this mechanism [8].

As it is possible to observe in the diffractograms, the spectra of PLA and PLA/PIL5 are identical, meaning that there is no evidence of the formation of SCs between PLA and poly(AEtMAC). A possible explanation is the low amount of poly(AEtMAC) that was mixed with PLA. Barbosa et al. [8] reported the formation of SCs of PLA and 5% wt of choline dihydrogen phosphate, a similar IL to poly(AEtMAC). However, the presence of SCs was much more evident when 20% wt of the IL was added.

3.7 Scanning electron microscopy

SEM analysis was performed in all samples, and the images can be observed in Figure 8, before and after the supercritical drying. All the membranes presented a similar morphology, but it is possible to notice that the membranes with SPIONs present larger rough areas and the membranes with poly(AEtMAC) present several white spots that indicate most likely its presence. However, these white spots are not observable in the PLA/PIL5 membrane. The presence of poly(AEtMAC) is far more noticeable in the scaffolds, where the white spots are clearly visible.

Fibre diameter was measured resorting to the software ImageJ 1.54d. PLA fibres show the largest diameter with a small increase with the supercritical drying. Although the sections taken of each sample constitute a very small fraction, it is possible to conclude that this drying process didn't affect fibre diameter, which is a plausible result since supercritical drying does not affect the fibre structure, as stated previously [14].

Table 1 summarizes the average diameter for each sample observed. PLA/PIL5 and PL/NP8 exhibit a small decrease in the fibre diameter upon supercritical drying, however, the fibres with the three components exhibited an 1.4-1.5-fold increase.

The morphology change from the membranes to the scaffolds is quite easy to notice. All the fibres of the scaffolds present much higher porosity than the membranes. Although in a much smaller scale, it is possible to produce nanofibres with pores via electrospinning in a

conventional setup without further treatment, as observed in Figure 8-E of PLA/PIL5/NP12 membrane. A possible explanation for this phenomenon is the phase separation mechanism [29]. The solvent used must be volatile (as DCM is) for it to completely and quickly evaporate during the deposition, leading to a phase separation between the polymer and the solvent. Thus, the areas rich in solvent will become porous regions after the evaporation. This mechanism by itself isn't enough to explain the formation of pores, otherwise, all the produced fibres in this work would present these features (such as most of all electrospun nanofibres). However, it is the basis of methods such as thermally induced phase separation and vapor induced phase separation, that can explain pore formation with a change in the environmental parameters of electrospinning.

Table 1 - Average fibre diameter before and after supercritical drying.

Sample	Membrane average diameter (nm)	Scaffold average diameter (nm)
PLA	801 ± 30	919 ± 230
PLA/PIL5	423 ± 112	383 ± 72
PLA/NP8	404 ± 50	386 ± 94
PLA/PIL5/NP8	332 ± 93	474 ± 85
PLA/PIL5/NP12	553 ± 86	836 ± 264

Several other works report the formation of porous PLA fibres. Natarajan et al. [37] produced porous fibres by increasing relative humidity and choosing a solvent with a high vapor pressure. The interaction between the solvent and the water led to pore formation.

Rezabeigi et al. [38], [39] used a ternary system, with hexane as nonsolvent, to fabricate porous nanofibres through phase separation, by the rapid evaporation of the solvent. In a humid environment, the water can also act as a nonsolvent. However, residual solvent was detected in the fibres and the induced porosity in the inside and at the surface was not coherent.

Still, resorting to techniques such as supercritical drying brings numerous benefits in the production of porous nanofibres for tissue engineering applications in a controlled manner. Supercritical drying is the most effective approach for producing aerogels with minimal structural collapse and it conserves better porous structures due to the fact that it avoids the liquid/gas boundary and consequently, there are no capillary forces that can damage pore structure [14].

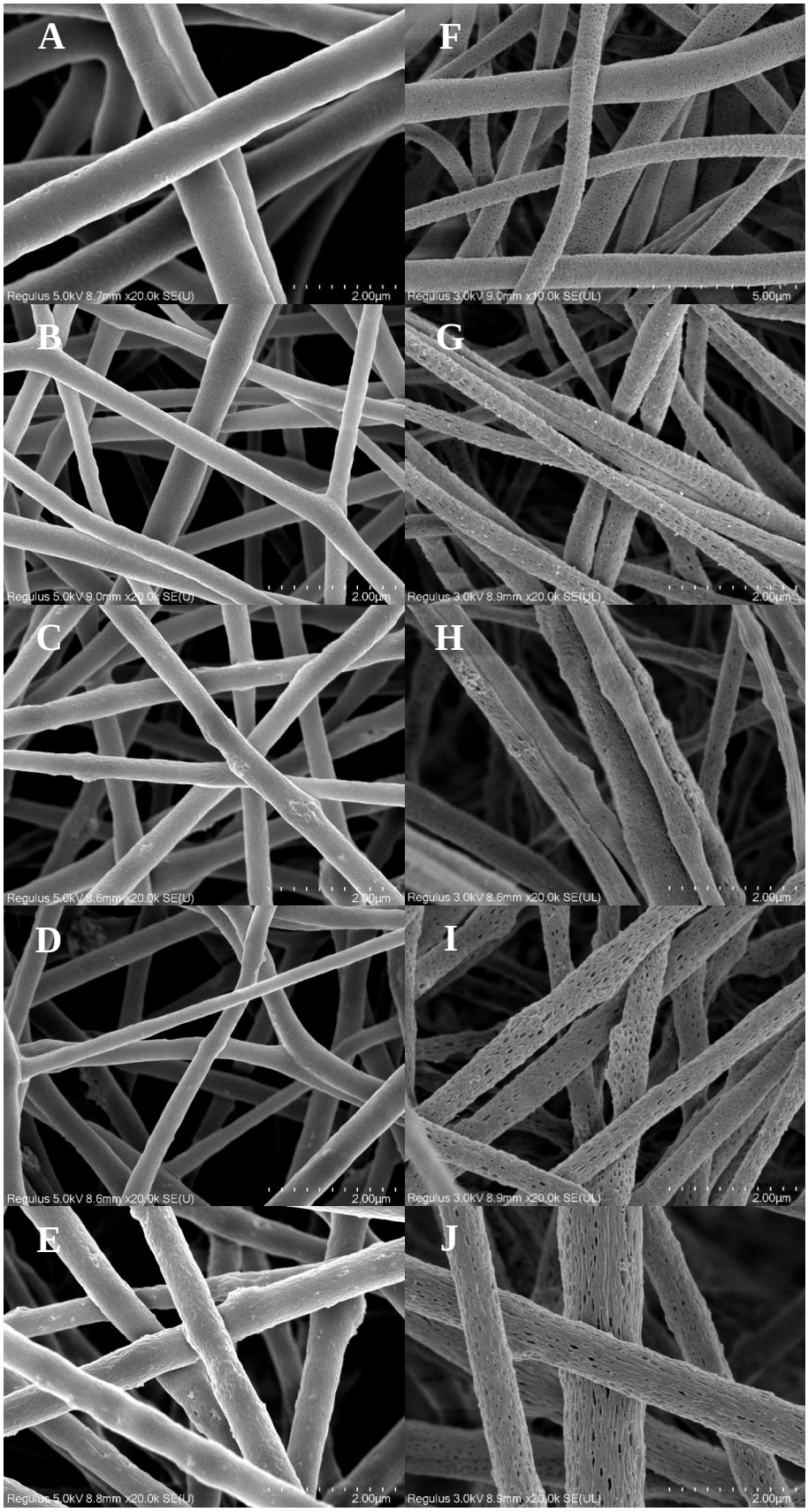

Figure 8 - SEM images of membranes A) PLA; B) PLA/PIL5; C) PLA/NP8; D) PLA/PIL5/NP8; E) PLA/PIL5/NP12 and scaffolds F) PLA; G)PLA/PIL5; H)PLA/NP8; I) PLA/PIL5/NP8; J) PLA/PIL/NP12.

According to IUPAC, pore sizes are classified in three different types: macropores (>50 nm), mesopores (2-50 nm) and micropores (<2 nm) [40], [41]. Individually, macroporosity promotes cell adhesion, growth, and infiltration, mesoporosity stimulates cell differentiation and proliferation, and microporosity enhances the metabolism. The interconnectivity between the different size pores contribute to the angiogenesis process, which is the growth mechanism of new blood vessels, essential for successful bone regeneration [6]. For tissue engineering purposes, another classification is commonly used, which divides pore sizes in macropores (>50 μm) and micropores (<50 μm) [41], a discrimination that is more suited to describe the bulk porosity of scaffolds.

In bones, porosity refers to the volume of empty spaces within the natural bone structure, while interconnectivity refers to the network of pores that are accessible outside the scaffold. As mentioned previously, the induction of porosity in BTE scaffolds is of utmost importance for bone tissue formation, as it controls cell proliferation and migration, as well as vascularization. Pore size influences the scaffold's efficiency. Smaller pores tend to increase cell differentiation rather than proliferation and larger ones tend to increase cell proliferation and vascularization of the new tissue, hence larger spaces supply more oxygen and nutrients to the inside of the scaffold. Macroporosity allows cell penetration and microporosity favours cell attachment. Both types of porosity, as well as pore interconnectivity, should co-exist in a BTE scaffold for a complete bone tissue regeneration [42].

In this work, only the fibre porosity was measured resorting to the software ImageJ, and so the classification used to analyse fibre porosity was IUPAC's. Mesoporosity was observed in all samples. The samples with SPIONs presented a few macropores, but no microporosity was detected in any sample. The average pore size varied between 20 and 30 nm for all the samples.

In order to measure the bulk porosity of the scaffolds, one could resort to techniques such as microcomputed tomography, liquid displacement or gravimetry [42].

3.8 Magnetic hyperthermia

Due to their superparamagnetic properties, SPIONs are a good candidate for cancer treatment [9]. Not only do they combine thermo and chemotherapy locally, but they also make the use of magnetic hyperthermia treatment possible. By applying an alternating magnetic field, local heating will be produced due to the absorbance power of SPIONs, reaching temperatures above 42ºC that will eliminate tumoral cells. Moreover, the magnetic system can be controlled at distance through the magnetic fields and their presence allows tracking of

drug release by MRI. It is also proven that SPIONs accelerate bone regeneration through a magnetic micro-environment, in which each NP creates a magnetic field that contributes to cell adhesion, proliferation and differentiation [12].

SPIONs were included in the membranes to take advantage of their superparamagnetic properties. Magnetic hyperthermia was performed during 10 minutes with the application of a 300 Gauss magnetic field, at a frequency of 388.4 Hz, only on the samples with SPIONs. The values of temperature variation and specific absorption rate (SAR) were calculated and are presented in the charts of Figure 9 and Figure 10.

Temperature variation is an important parameter when performing magnetic hyperthermia treatment due to the possibility of localized cancer treatment. Tumoral cells are more sensitive to high temperature than healthy cells, therefore maintaining the temperature near the tumour above 42ºC enough time will eliminate tumoral cells [9]. As the human body normal temperature is around 37ºC, a temperature variation of 5ºC would be enough to reach the critical temperature to eliminate tumoral cells. As seen in Figure 9, all the samples registered a temperature variation above 5ºC, which means that they are suited for magnetic hyperthermia for cancer treatment. The samples PLA/PIL5/NP12 registered the highest increase in temperature, as they had the higher content in SPIONs. It is also possible to verify that only in PLA/PIL5/NP12, the scaffold registered a higher temperature variation than the membrane, meaning that the supercritical drying made more difference in the membrane with higher content in SPIONs, as in the other two samples there was no significant change noticed.

SAR is a parameter that quantifies the power absorbed by the magnetic material per unit of mass, and it is a measure of the heating efficiency of the SPIONs. It is calculated through the following expression [18], [43]:

$$SAR\ (Wg^{-1}) = \frac{C_{NP} \cdot m_{Fe} + C_l \cdot m_l}{m_{Fe}} \cdot \left(\frac{dT}{dt}\right)_{max}$$

where C_{NP} and C_l are the specific heat capacity of the SPIONs and water, respectively, m_{Fe} and m_l are the masses of SPIONs and water, respectively, and $\left(\frac{dT}{dt}\right)_{max}$ is the slope in the first seconds of the experimental curve, when the membrane is under adiabatic conditions [43].

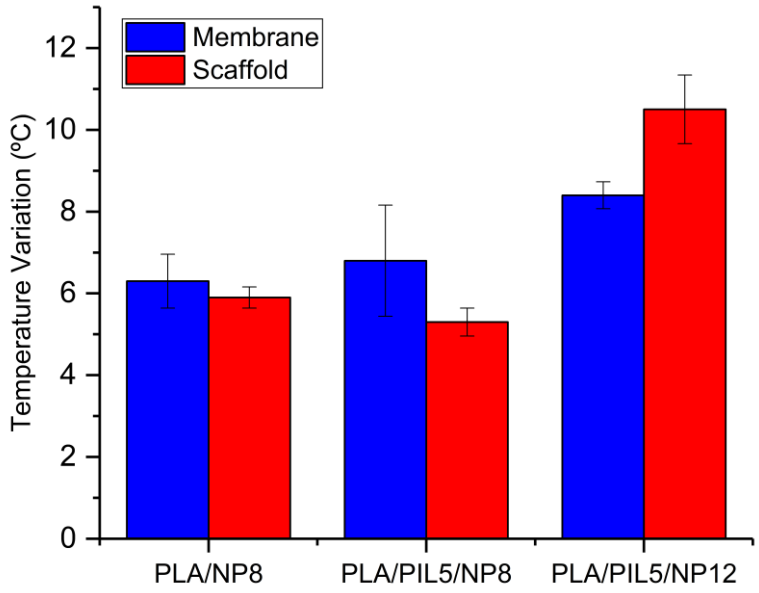

Figure 9 - Temperature variation of the samples after magnetic hyperthermia assays.

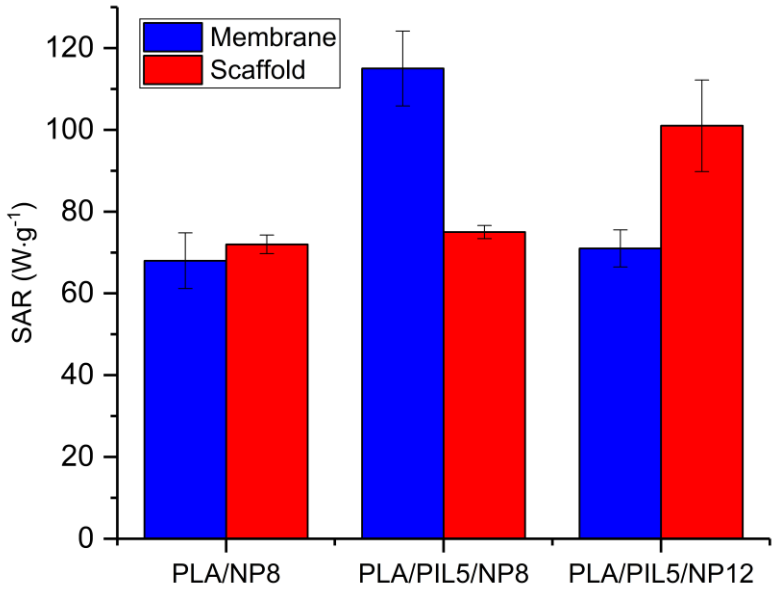

Figure 10 - SAR values of the samples after magnetic hyperthermia assays.

Figure 10 shows the calculated SAR values for the samples with SPIONs. The values of temperature variation and SAR of all samples can be consulted in Table 2. It is possible to observe that the values of PLA/NP8 sample are identical. However, the PLA/PIL5/NP8 membrane presents a higher value than the scaffold, opposite to what is verified regarding the PLA/PIL5/NP12 sample. This result corroborates the temperature variation one, also concluding that the supercritical drying has a better impact in the sample with 12% wt SPIONs for magnetic hyperthermia treatment, possibly due to an increase in the effectiveness of this amount of

SPIONS to produce hyperthermia in more porous samples, due better accessibility of water [44].

Table 2 - Temperature variation and SAR values of the membranes and scaffolds

Sample		Temperature variation (ºC)	SAR (Wg^{-1})
PLA/NP8	Membrane	6.30 ± 0.66	68.0 ± 6.8
	Scaffold	5.90 ± 0.26	72.0 ± 2.3
PLA/PIL5/NP8	Membrane	6.80 ± 1.36	115.0 ± 9.2
	Scaffold	5.30 ± 0.34	75.0 ± 1.6
PLA/PIL5/NP12	Membrane	8.40 ± 0.33	71.0 ± 4.6
	Scaffold	10.50 ± 0.84	101.0 ± 11.2

3.9 Cytotoxicity assays

Cell viability was tested with a human osteosarcoma cell line (Saos-2) and the results are presented in Figure 11. According to ISO 10993-5, a cell viability above 80% means that the samples do not present cytotoxicity [45]. For all the samples and for all the extract concentrations, cell viability percentage is above 94%, which indicates that no sample is cytotoxic, thus the produced materials can be considered for BTE applications.

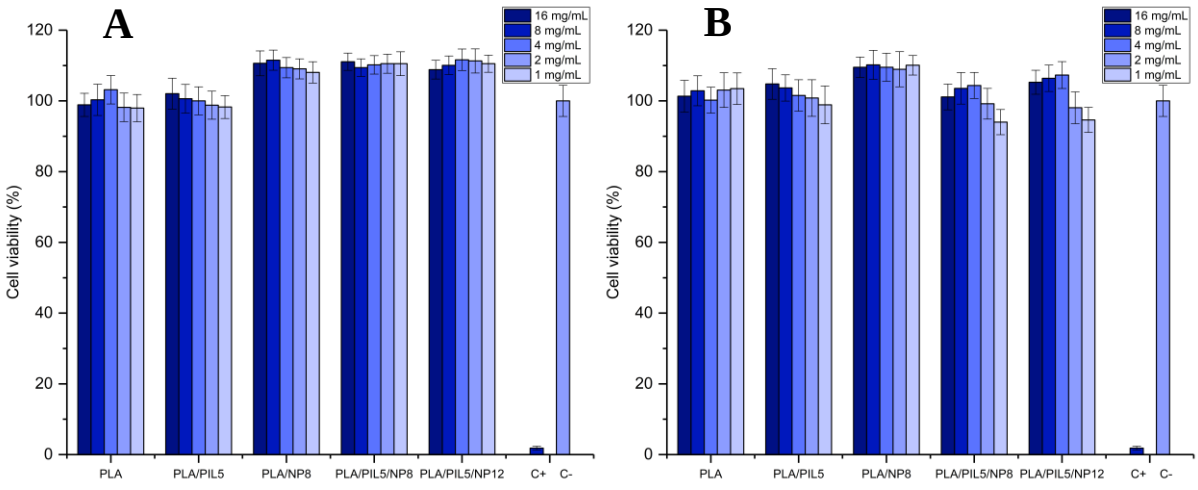

Figure 11 - Results of Saos-2 cells' viability obtained for the membranes (A) and scaffolds (B).

4

CONCLUSIONS AND FUTURE PERSPECTIVES

This project aimed to develop new polymeric fibrous membranes for BTE applications, relying on a cholinium-based poly(IL) and SPIONs to enhance its performance. Its production involved electrospinning for the fabrication of the nanofibres and supercritical drying with CO_2 to induce porosity in the fibres. Non-dried and dried membranes were characterized and tested for its cytotoxicity with Saos-2.

The obtained results show that supercritical drying induced the wanted porosity in the fibres, which probably will turn these materials more suitable for biomedical applications, since porosity foments the biological processes of tissue regeneration. This treatment also enhanced the crystallinity. However, there isn't any evidence of the formation of SCs between PLA and poly(AEtMAC), which leads us to believe that a higher amount of that compound should have been added for SCs to be detected.

Two different concentrations of SPIONs were tested: 8 and 12% wt. The magnetic hyperthermia results show that the membrane with 12% wt presented a larger temperature increase, important for local cancer treatment. On top of that, it was the only membrane that presented a higher temperature variation and SAR after the supercritical drying, meaning that this treatment had better impact in the membrane with higher content in SPIONs.

Regarding cell viability assays, no sample presented cytotoxicity for Saos-2, which means that all the produced membranes can be considered for tissue engineering applications. It is important to emphasize that the samples with 12% wt SPIONs are also non-cytotoxic, meaning that SPIONs concentration could potentially be increased for better results in magnetic hyperthermia while remaining non-cytotoxic.

The obtained results are promising, but some tests could still be done to know better the full potential of these materials for BTE purposes. It would be important to measure the bulk porosity of the membranes to find out if cells could adhere and develop for successful bone tissue regeneration, by resorting to techniques such as microcomputed tomography, liquid displacement or gravimetry.

Several *in vitro* tests can be used to assess the behaviour of the cells when in contact with the material. The most suited tests for the continuation of this work are cell attachment,

proliferation, and cell differentiation assays, as the results would show if the porosity and the interconnectivity of the produced materials are appropriated for bone tissue regeneration.

As research and science continue to evolve, it is expected to see even more innovative and effective BTE treatments emerge in the years to come. With the adoption of BTE as the main method for the treatment of bone injuries and diseases, it is possible to envision a future where everyone has the opportunity to live a healthy and fulfilling life, regardless of their age or medical condition.

5 BIBLIOGRAPHY

[1] R. Langer and J. P. Vacanti, "Tissue Engineering," *Science*, vol. 260, no. 5110, pp. 920–926, May 1993, doi: 10.1126/science.8493529.

[2] J. P. Vacanti, "Beyond Transplantation," *Archives of Surgery*, vol. 123, no. 5, p. 545, May 1988, doi: 10.1001/archsurg.1988.01400290027003.

[3] P. S. Russell, "Selective Transplantation," *Ann Surg*, vol. 201, no. 3, pp. 255–262, Mar. 1985, doi: 10.1097/00000658-198503000-00001.

[4] H. Qu, H. Fu, Z. Han, and Y. Sun, "Biomaterials for bone tissue engineering scaffolds: a review," *RSC Adv*, vol. 9, no. 45, pp. 26252–26262, 2019, doi: 10.1039/C9RA05214C.

[5] R. Florencio-Silva, G. R. da S. Sasso, E. Sasso-Cerri, M. J. Simões, and P. S. Cerri, "Biology of Bone Tissue: Structure, Function, and Factors That Influence Bone Cells," *Biomed Res Int*, vol. 2015, pp. 1–17, 2015, doi: 10.1155/2015/421746.

[6] M. N. Collins, G. Ren, K. Young, S. Pina, R. L. Reis, and J. M. Oliveira, "Scaffold Fabrication Technologies and Structure/Function Properties in Bone Tissue Engineering," *Adv Funct Mater*, vol. 31, no. 21, p. 2010609, May 2021, doi: 10.1002/adfm.202010609.

[7] S. A. Forsyth, J. M. Pringle, and D. R. MacFarlane, "Ionic Liquids—An Overview," *Aust J Chem*, vol. 57, no. 2, p. 113, 2004, doi: 10.1071/CH03231.

[8] P. Barbosa, J. Campos, A. Turygin, V. Y. Shur, A. Kholkin, A. Barros-Timmons and F. M. Figueiredo, "Piezoelectric poly(lactide) stereocomplexes with a cholinium organic ionic plastic crystal," *J Mater Chem C Mater*, vol. 5, no. 46, pp. 12134–12142, 2017, doi: 10.1039/C7TC03484A.

[9] P. I. P. Soares and J. P. Borges, "Recent advances in magnetic electrospun nanofibers for cancer theranostics application," *Progress in Natural Science: Materials International*, vol. 31, no. 6, pp. 835–844, Dec. 2021, doi: 10.1016/j.pnsc.2021.11.003.

[10] S. Nemati, S. Kim, Y. M. Shin, and H. Shin, "Current progress in application of polymeric nanofibers to tissue engineering," *Nano Converg*, vol. 6, no. 1, p. 36, Dec. 2019, doi: 10.1186/s40580-019-0209-y.

[11] H. Hajiali, L. Ouyang, V. Llopis-Hernandez, O. Dobre, and F. R. A. J. Rose, "Review of emerging nanotechnology in bone regeneration: progress, challenges, and perspectives," *Nanoscale*, vol. 13, no. 23, pp. 10266–10280, Jun. 2021, doi: 10.1039/D1NR01371H.

[12] C. Shuai, W. Yang, C. He, S. Peng, C. Gao, Y. Yang, F. Qi, P. Feng "A magnetic micro-environment in scaffolds for stimulating bone regeneration," *Mater Des*, vol. 185, p. 108275, Jan. 2020, doi: 10.1016/j.matdes.2019.108275.

[13] C. A. García-González, M. C. Camino-Rey, M. Alnaief, C. Zetzl, and I. Smirnova, "Supercritical drying of aerogels using CO2: Effect of extraction time on the end material textural properties," *J Supercrit Fluids*, vol. 66, pp. 297–306, Jun. 2012, doi: 10.1016/j.supflu.2012.02.026.

[14] Z. Sheng, Z. Liu, Y. Hou, H. Jiang, Y. Li, G. Li, X. Zhang, "The Rising Aerogel Fibers: Status, Challenges, and Opportunities," *Advanced Science*, vol. 10, no. 9, p. 2205762, Mar. 2023, doi: 10.1002/advs.202205762.

[15] E. B. Yahya, A. A. Amirul, Abdul Khalil H. P. S., N. G. Olaiya, M. O. Iqbal, F. Jummat, Atty Sofea A. K. and A. S. Andan, "Insights into the Role of Biopolymer Aerogel Scaffolds in Tissue Engineering and Regenerative Medicine," *Polymers (Basel)*, vol. 13, no. 10, p. 1612, May 2021, doi: 10.3390/polym13101612.

[16] B. Pan, J. Lei, L. Zhang, and Y. Guo, "Research on the physical properties of supercritical CO2 and the log evaluation of CO2-bearing volcanic reservoirs," *Journal of Geophysics and Engineering*, vol. 14, no. 5, pp. 1052–1060, Oct. 2017, doi: 10.1088/1742-2140/aa6f22.

[17] L. Zheng, S. Zhang, Z. Ying, J. Liu, Y. Zhou, and F. Chen, "Engineering of Aerogel-Based Biomaterials for Biomedical Applications," *Int J Nanomedicine*, vol. Volume 15, pp. 2363–2378, Apr. 2020, doi: 10.2147/IJN.S238005.

[18] P. I. P. Soares, C. A. T. Laia, A. Carvalho, L. C. J. Pereira, J. T. Coutinho, I. M. M. Ferreira, C. M. M. Novo and J. P. Borges, "Iron oxide nanoparticles stabilized with a bilayer of oleic acid for magnetic hyperthermia and MRI applications," *Appl Surf Sci*, vol. 383, pp. 240–247, Oct. 2016, doi: 10.1016/j.apsusc.2016.04.181.

[19] M. Isik, R. Gracia, L. C. Kollnus, L. C. Tomé, I. M. Marrucho, and D. Mecerreyes, "Cholinium-Based Poly(ionic liquid)s: Synthesis, Characterization, and Application as Biocompatible Ion Gels and Cellulose Coatings," *ACS Macro Lett*, vol. 2, no. 11, pp. 975–979, Nov. 2013, doi: 10.1021/mz400451g.

[20] P. I. P. Soares, J. Romão, R. Matos, J. C. Silva, and J. P. Borges, "Design and engineering of magneto-responsive devices for cancer theranostics: Nano to macro perspective," *Prog Mater Sci*, vol. 116, p. 100742, Feb. 2021, doi: 10.1016/j.pmatsci.2020.100742.

[21] M. S. Singhvi, S. S. Zinjarde, and D. V. Gokhale, "Polylactic acid: synthesis and biomedical applications," *J Appl Microbiol*, vol. 127, no. 6, pp. 1612–1626, Dec. 2019, doi: 10.1111/jam.14290.

[22] B. Chieng, N. Ibrahim, W. Yunus, and M. Hussein, "Poly(lactic acid)/Poly(ethylene glycol) Polymer Nanocomposites: Effects of Graphene Nanoplatelets," *Polymers (Basel)*, vol. 6, no. 1, pp. 93–104, Dec. 2013, doi: 10.3390/polym6010093.

[23] J. P. Mofokeng, A. S. Luyt, T. Tábi, and J. Kovács, "Comparison of injection moulded, natural fibre-reinforced composites with PP and PLA as matrices," *Journal of Thermoplastic Composite Materials*, vol. 25, no. 8, pp. 927–948, Dec. 2012, doi: 10.1177/0892705711423291.

[24] S.-U. Zhang, "Classifying Degraded Three-Dimensionally Printed Polylactic Acid Specimens Using Artificial Neural Networks based on Fourier Transform Infrared Spectroscopy," *Applied Sciences*, vol. 9, no. 13, p. 2772, Jul. 2019, doi: 10.3390/app9132772.

[25] D. V. Morales, B. L. Rivas, and N. Escalona, "Poly([(2-methacryloyloxy)ethyl]trimethylammonium chloride): synthesis, characterization, and removal properties of As(V)," *Polymer Bulletin*, vol. 73, no. 3, pp. 875–890, Mar. 2016, doi: 10.1007/s00289-015-1524-z.

[26] C.-G. Lee and J.-H. Kim, "Improved drying method for removal of residual solvents from paclitaxel by pre-treatment with ethanol and water," *Process Biochemistry*, vol. 50, no. 6, pp. 1031–1036, Jun. 2015, doi: 10.1016/j.procbio.2015.02.018.

[27] K. Grodowska and A. Parczewski, "Organic solvents in the pharmaceutical industry.," *Acta Pol Pharm*, vol. 67, no. 1, pp. 3–12, 2010, [Online]. Available: http://www.ncbi.nlm.nih.gov/pubmed/20210074

[28] K. Li, Z. Yingnan, X. Junwei, W. Jingxi, G. Xuenan, L. Ping and F. Yubo "Three-dimensional magnetic fibrous scaffold with icariin expanded by supercritical CO2 for bone tissue engineering under static magnetic field," *Compos B Eng*, vol. 226, p. 109304, Dec. 2021, doi: 10.1016/j.compositesb.2021.109304.

[29] C. Huang and N. L. Thomas, "Fabrication of porous fibers via electrospinning: strategies and applications," *Polymer Reviews*, vol. 60, no. 4, pp. 595–647, Oct. 2020, doi: 10.1080/15583724.2019.1688830.

[30] P. Chocholata, V. Kulda, and V. Babuska, "Fabrication of Scaffolds for Bone-Tissue Regeneration," *Materials*, vol. 12, no. 4, p. 568, Feb. 2019, doi: 10.3390/ma12040568.

[31] M. Mihai, M. A. Huneault, and B. D. Favis, "Crystallinity development in cellular poly(lactic acid) in the presence of supercritical carbon dioxide," *J Appl Polym Sci*, vol. 113, no. 5, pp. 2920–2932, Sep. 2009, doi: 10.1002/app.30338.

[32] R. Moussaoui, K. Elghniji, M. ben Mosbah, E. Elaloui, and Y. Moussaoui, "Sol–gel synthesis of highly TiO2 aerogel photocatalyst via high temperature supercritical drying," *Journal of Saudi Chemical Society*, vol. 21, no. 6, pp. 751–760, Sep. 2017, doi: 10.1016/j.jscs.2017.04.001.

[33] W. Mo, F. Kong, K. Chen, and B. Li, "Relationship between freeze-drying and supercritical drying of cellulosic fibers with different moisture contents based on pore and crystallinity measurements," *Wood Sci Technol*, vol. 56, no. 3, pp. 867–882, May 2022, doi: 10.1007/s00226-022-01387-w.

[34] H. Kaczmarek, M. Nowicki, I. Vuković-Kwiatkowska, and S. Nowakowska, "Crosslinked blends of poly(lactic acid) and polyacrylates: AFM, DSC and XRD studies," *Journal of Polymer Research*, vol. 20, no. 3, p. 91, Mar. 2013, doi: 10.1007/s10965-013-0091-y.

[35] S. Pandey, S. Neupane, D. K. Gupta, R. J. Yadav, and A. P. Yadav, "Synthesis and application of Fe3O4 nanoparticles in electrochemical pseudocapacitor," *Emergent Mater*, vol. 5, no. 6, pp. 1899–1906, Dec. 2022, doi: 10.1007/s42247-022-00417-4.

[36] Y. Jing, C. Quan, B. Liu, Q. Jiang, and C. Zhang, "A Mini Review on the Functional Biomaterials Based on Poly(lactic acid) Stereocomplex," *Polymer Reviews*, vol. 56, no. 2, pp. 262–286, Apr. 2016, doi: 10.1080/15583724.2015.1111380.

[37] L. Natarajan, J. New, A. Dasari, S. Yu, and M. A. Manan, "Surface morphology of electrospun PLA fibers: mechanisms of pore formation," *RSC Adv.*, vol. 4, no. 83, pp. 44082–44088, 2014, doi: 10.1039/C4RA06215A.

[38] E. Rezabeigi, M. Sta, M. Swain, J. McDonald, N. R. Demarquette, R. A. L. Drew and P. M. Wood-Adams, "Electrospinning of porous polylactic acid fibers during nonsolvent induced phase separation," *J Appl Polym Sci*, vol. 134, no. 20, May 2017, doi: 10.1002/app.44862.

[39] E. Rezabeigi, P. M. Wood-Adams, and N. R. Demarquette, "Complex Morphology Formation in Electrospinning of Binary and Ternary Poly(lactic acid) Solutions," *Macromolecules*, vol. 51, no. 11, pp. 4094–4107, Jun. 2018, doi: 10.1021/acs.macromol.8b00083.

[40] R. Liu, L. Hou, G. Yue, H. Li, J. Zhang, J. Liu, B. Miao, N. Wang, J. Bai, Z. Cui, T. Liu and Y. Zhao, "Progress of Fabrication and Applications of Electrospun Hierarchically Porous

Nanofibers," *Advanced Fiber Materials*, vol. 4, no. 4, pp. 604–630, Aug. 2022, doi: 10.1007/s42765-022-00132-z.

[41] R. A. Perez and G. Mestres, "Role of pore size and morphology in musculo-skeletal tissue regeneration," *Materials Science and Engineering: C*, vol. 61, pp. 922–939, Apr. 2016, doi: 10.1016/j.msec.2015.12.087.

[42] H. Mohammadi, M. Sepantafar, N. Muhamad, and A. Bakar Sulong, "How Does Scaffold Porosity Conduct Bone Tissue Regeneration?," *Adv Eng Mater*, vol. 23, no. 10, Oct. 2021, doi: 10.1002/adem.202100463.

[43] P. I. P. Soares, D. Machado, C. A. T. Laia, L. C. J. Pereira, J. T. Coutinho, I. M. M. Ferreira, C. M. M. Novo and J. P. Borges, "Thermal and magnetic properties of chitosan-iron oxide nanoparticles," *Carbohydr Polym*, vol. 149, pp. 382–390, Sep. 2016, doi: 10.1016/j.carbpol.2016.04.123.

[44] A. Adam, K. Parkhomenko, P. Duenas-Ramirez, C. Nadal, G. Cotin, P.-E. Zorn, P. Choquet, S. Bégin-Colin and D. Mertz, "Orienting the Pore Morphology of Core-Shell Magnetic Mesoporous Silica with the Sol-Gel Temperature. Influence on MRI and Magnetic Hyperthermia Properties," *Molecules*, vol. 26, no. 4, p. 971, Feb. 2021, doi: 10.3390/molecules26040971.

[45] J. López-García, M. Lehocký, P. Humpolíček, and P. Sáha, "HaCaT Keratinocytes Response on Antimicrobial Atelocollagen Substrates: Extent of Cytotoxicity, Cell Viability and Proliferation," *J Funct Biomater*, vol. 5, no. 2, pp. 43–57, May 2014, doi: 10.3390/jfb5020043.

[46] A. Keirouz, Z. Wang, V. S. Reddy, Z. K. Nagy, P. Vass, M. Buzgo, S. Ramakrishna and N. Radacsi, "The History of Electrospinning: Past, Present, and Future Developments," *Adv Mater Technol*, vol. 8, no. 11, Jun. 2023, doi: 10.1002/admt.202201723.

[47] T. Vieira, J. Carvalho Silva, A. M. Botelho do Rego, J. P. Borges, and C. Henriques, "Electrospun biodegradable chitosan based-poly(urethane urea) scaffolds for soft tissue engineering," *Materials Science and Engineering: C*, vol. 103, p. 109819, Oct. 2019, doi: 10.1016/j.msec.2019.109819.

A
APPENDIX

A.1 Literature revision

It is possible to adjust the properties of the fibres by changing the electrospinning setup. An example is co-axial electrospinning, which consists of two aligned needles that eject two different solutions and produce fibres encapsulated by other fibres, the so-called core-shell nanofibres. Centrifugal electrospinning unites the principles of electrospinning and centrifugal spinning. In this process, spinning occurs in a rotating disc with several spinnerets due to the centrifugal force acting on the jet. The needleless electrospinning technique is another novel alternative that improves process productivity and quality of the fibres. An example of a needleless process is roller electrospinning, that resorts to a rotating cylinder electrode submerged in a polymeric solution with continuous airflow. A thin layer of polymer is formed on the cylinder's surface, and it is ejected when a high voltage is applied [46].

Both natural and synthetic polymers can be utilized to produce scaffolds for tissue engineering, and each one has its pros and cons. Synthetic polymers are better for processing and their mechanical properties can adequately be tuned. On the other hand, natural polymers possess innate bioactivity and give rise to scaffolds with better cell attachment, proliferation, and differentiation. On top of that, the degradation products of natural polymers aren't injurious and trigger a low immunological response, as some of them are already found in the human body, including in bone tissue [10].

According to Nemati et al. [10], several synthetic polymers have already been electrospun for tissue engineering applications, such as PCL, PGA, and PLA. PCL is a good candidate for applications requiring high mechanical resistance, while PGA and PLA (as well as the copolymer poly(lactic-co-glycolic acid) (PLGA)) are suited for applications that call for higher degradation rates and natural degradation products.

Table A1 - Characteristics, advantages and disadvantages of some biomaterials used for BTE. Adapted from [4], [6].

Material type	Biomaterial	Characteristics	Advantages	Disadvantages
Metals	Ti-alloys	Durable, biocompatible, resistant to corrosion	High bone affinity	Non-biodegradable
Bioceramics	HAp	Main inorganic component of bone	Biocompatible, non-toxic, osteoinductive and osteoconductive	Low mechanical strength and resorption rate
	β-TCP	Similar Ca/P rate to natural bone tissue	Biocompatible, highly resorbable	Brittle, inconsistent degradation rate
Natural polymers	Collagen	Organic component of bone	Biodegradable, different forms of scaffolds, non-cytotoxic	Complex structure, difficult disinfection and handling
	Gelatin	Denatured collagen	Biocompatible, biodegradable	Low mechanical properties
	Chitosan	Polysaccharide insoluble in water	Biodegradable	
Synthetic polymers	PCL	Crystalline polymer	Good mechanical properties, biocompatible, biodegradable	Slow degradation rate
	PLA, PGA	Approved by the U.S. FDA for biomedical applications	Natural degradation products, biocompatible, biodegradable, good mechanical properties	Slow degradation rate, shortage of cell adhesion

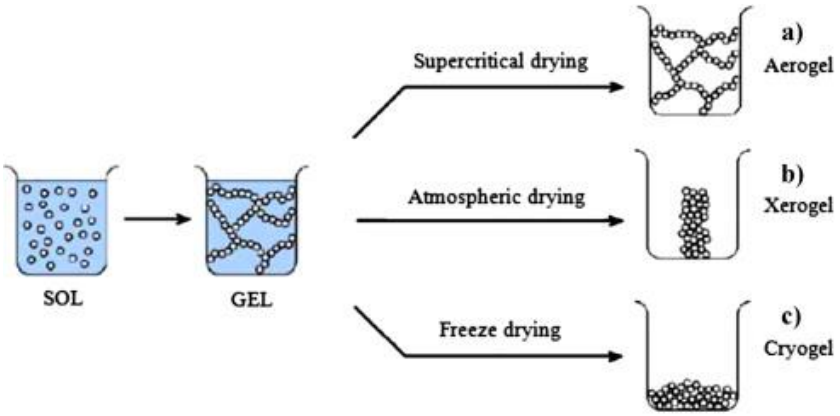

Figure A1 - Drying methodologies to produce gels: a) supercritical drying; b) atmospheric drying; c) freeze drying. Retrieved from [13].

A.2 Materials

Polylactic acid Luminy D120 ($C_3H_4O_2$, M_W=120 kg/mol) was obtained from Corbion. Iron (II) chloride tetrahydrate, 98% ($FeCl_2{\cdot}4H_2O$, CAS 13478-10-9) was obtained from Thermo Scientific. Iron (III) chloride hexahydrate, 97% ($FeCl_3{\cdot}6H_2O$, CAS 10025-77-1) was obtained from Alfa Aesar. Ammonium hydroxide aqueous solution, 28-30% (NH_4OH, CAS 1336-21-6) was obtained from Honeywell. Oleic acid ($C_{18}H_{34}O_2$, CAS 112-80-1) was obtained from Fisher Chemical. [2-(Acryloyloxy)-ethyl] trimethylammonium chloride aqueous solution, 80% ($C_8H_{16}ClNO_2$, CAS 44992-01-0) was obtained from Sigma-Aldrich. 2,2'-Azobis(2-methyl-propionamidine) dihydrochloride 97% ($C_8H_{20}Cl_2N_6$, CAS 2997-92-4) was obtained from Sigma-Aldrich. Dichloromethane (CH_2Cl_2, CAS 75-09-2) was obtained from Sigma-Aldrich. *N, N*-Dimethylformamide (C_3H_7NO, CAS 68-12-2) was obtained from Fisher Chemical. Ultrapure water was used for the synthesis of the SPIONs and poly(AEtMAC). Ethanol 99.8% from Honeywell (C_2H_5OH, CAS 64-17-5) was used for the supercritical drying. The CO_2 (> 99.9%) was purchased from Air Liquide S.A.. Deuterated water, 98% (D_2O) from Eurisotop was used for NMR experiments. For the cytotoxicity assays, McCoy's 5A medium from Sigma-Aldrich (#M4892), resazurin from Alfa Aesar (in a 0.2 mg/mL concentration in PBS) and dimethyl sulfoxide (DMSO) from Merck (C_2H_6OS, CAS 67-68-5) were used.

A.3 Characterization

ATR-FTIR: The membrane chemical structure was analysed using ATR-FTIR spectroscopy in a Perkin Elmer Spectrum Two FTIR spectrometer. The spectra were obtained in the range of 4000 to 400 cm^{-1} with 16 scans.

TGA: Thermal decomposition of the samples and of poly(AEtMAC) was measured in a thermogravimetric Analyzer Setaram Labsys EVO from room temperature to 500ºC at a rate of 10ºC/min.

NMR: NMR data were acquired at 298.2 K in a Bruker Avance III 400 spectrometer functioning at 400.15 MHz Larmor frequency for hydrogen. ^{1}H NMR experiments were acquired with 64 K time domain points over a spectral window of 8012.820 Hz (20.0244 ppm) centred at 2471.09 Hz (6.175 ppm) and with 16 scans per FID; the relaxation delay was set in 5.0 s. Data was processed using Bruker Topspin 3.6.2 software.

XRD: X-ray diffraction was used to analyse the phase composition of the membranes, resorting to a PANalytical Xpert PRO MRD diffractometer with a Cu anode. The samples were measured from 10º to 90º. After analysing the electrospun membranes, the samples were submitted to supercritical drying and analysed again.

SEM: Fibre morphology and diameter were analysed by a Hitachi Regulus SU8220 scanning electron microscope. The average diameter and pore size were measured with the software ImageJ version 1.54d.

Magnetic hyperthermia: The response of the SPIONs to an external magnetic field was quantified using magnetic hyperthermia technique in D5 series equipment from nB nanoscale Biomagnetics. These assays were performed only in the membranes with SPIONs (non-dried and dried) and 3 tests with 20 mg of membrane were made for each sample. The measurements took 10 minutes and the magnetic flux density and frequency used were respectively 300 Gauss and 388.4 kHz.

Cytotoxicity: Cytotoxicity was studied for the Saos-2 in McCoy's 5A medium. The *in vitro* cytotoxicity by extract method [47] was performed according to the International Standard ISO 10993-5 "Biological evaluation of medical devices—Part 5: Tests for in vitro cytotoxicity".

A.4 Electrospinning

Table A2 - Content of the solutions for electrospinning.

Solution	PLA (% wt)	poly(AEtMAC) (% wt)	SPIONs (% wt)
PLA	10	-	-
PLA/PIL5	10	5	-
PLA/NP8	10	-	8
PLA/PIL5/NP8	10	5	8
PLA/PIL5/NP12	10	5	12

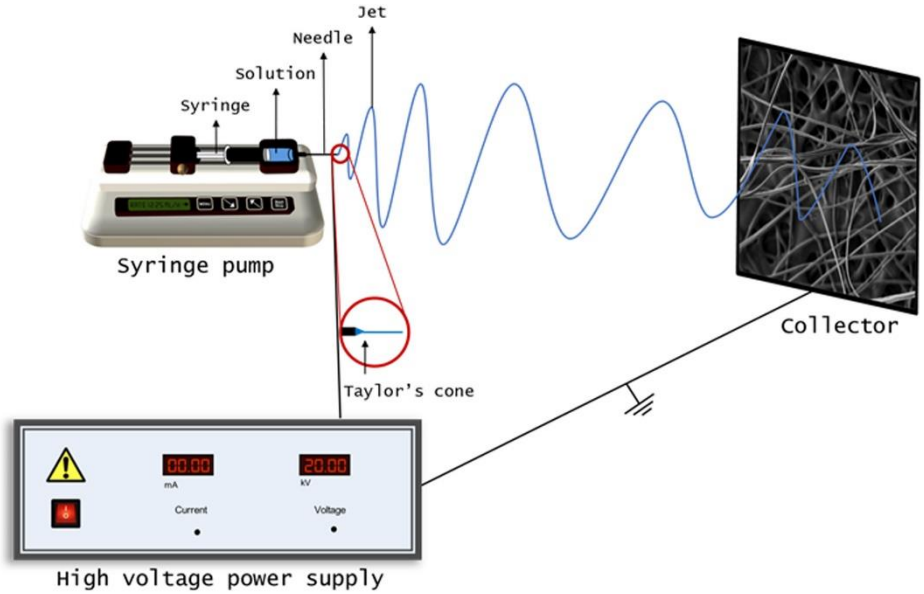

Figure A2 - Schematic of the electrospinning setup used. Retrieved from [20].

Table A3 - Electrospinning parameters.

Membrane	Flow rate (mL/h)	Voltage (kV)	Distance (cm)	Temperature (°C)	Relative humidity (%)
PLA	0.5	22	15	18.5	36
PLA/PIL5	0.5	20	15	20.5	42
PLA/NP8	0.3	20	15	21.0	45
PLA/PIL5/NP8	0.3	20	15	21.5	42
PLA/PIL5/NP12	0.3	20	15	21.0	42

A.5 Supercritical drying

In this project, the fluid used for supercritical drying was CO_2, which reaches its supercritical point at a temperature and pressure of 31.06 ºC and 73.9 bar, respectively [16].

The first drying attempt was performed by placing dry ice in contact with the membranes in a closed vessel, as reported by Li et al. [28].

The equipment used for supercritical drying is described in Figure A3, and the respective caption is in Table A4. It is important to mention that the cell is inside an oven. After putting the membranes inside Whatman paper cartridges and immersing them in ethanol, they are placed inside the 300 mL cell with 100 mL of ethanol. The cell is then placed in its position (C-1) and the thermostatic bath is turned on. Then, all the valves are closed, and the oven temperature is set at 42 ºC. After checking if there isn't any overheating of the system, the CO_2 cylinder is fully opened slowly. V-1 is fully opened slowly, the pump pressure is checked. When the system is stable, V-3 is fully opened slowly, and it's verified if there are any leaks in the cell. Finally, the BPR is reduced, and V-4 is fully opened slowly. After the stabilization of the system at 120 bar, all valves are closed, as well the CO_2 cylinder.

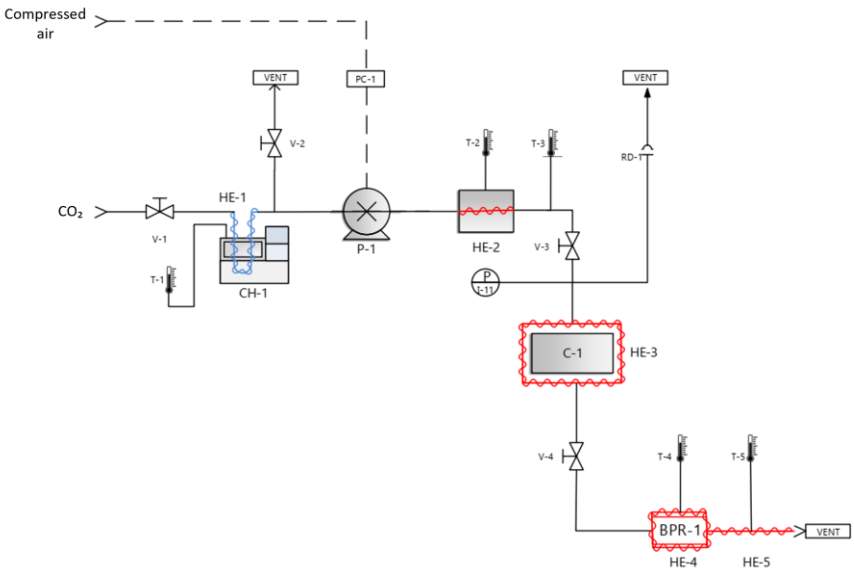

Figure A3 - Schematic of the supercritical drying assembly.

Table A4 - Caption of the supercritical drying assembly.

BPR-1	Back pressure regulator
CH-1	Thermostatic bath
C-1	Drying cell
HE-1	Heat permutator
HE-2-5	Heating resistance
T-1-5	Temperature sensor
V-1-4	Needle valve
RD-1	Rupture disc
PC-1	Pressure regulator

After this first long cycle in batch that took 24 hours, 3 more shorter cycles were performed. The first flow cycle to make CO_2 leave the cell took 2 hours at 120 bar. For this cycle, V-3 and V-4 were opened. Then, a batch cycle is performed with V-3 and V-4 closed to force the remaining CO_2 to mix with the ethanol took 30 minutes at 120 bar The last flow cycle also took 30 minutes at 120 bar, followed by 20 minutes of depressurization, where BPR is slowly opened so that the pressure slowly decreases. The membranes were removed from the cell 24 hours later.

A.6 Cytotoxicity assays

Cytotoxicity assays were performed according to ISO 10993-5, "Biological evaluation of medical devices: tests for *in vitro* cytotoxicity", by the extract method.

The extracts were prepared after sample sterilization at 120 ºC, by placing the samples in McCoy's 5A medium at 37ºC for at least 24 hours. The cells were placed in a 96-well plate and incubated at 37ºC for 24 hours. Then, the medium was replaced by the extracts in different concentrations, ranging from 16 mg/mL to 1 mg/mL and incubated again at 37ºC for 48 hours. Five replicas for each concentration were used for all samples. After that, the medium was again replaced by a solution with medium and resazurin (50:50), which acts as a cell viability indicator. Viable cells reduce resazurin to resorufin, translating in a different absorbance value from 600 to 570 nm (absorption peaks of resazurin and resorufin, respectively). That difference is proportional to cell viability. For each group of samples (membranes and scaffolds), two control groups were made. A negative one consisted only of cells placed in the medium and a positive one, consisted of adding 10 µL of DMSO, killing all cells in those wells [47].

A.7 X-ray diffraction

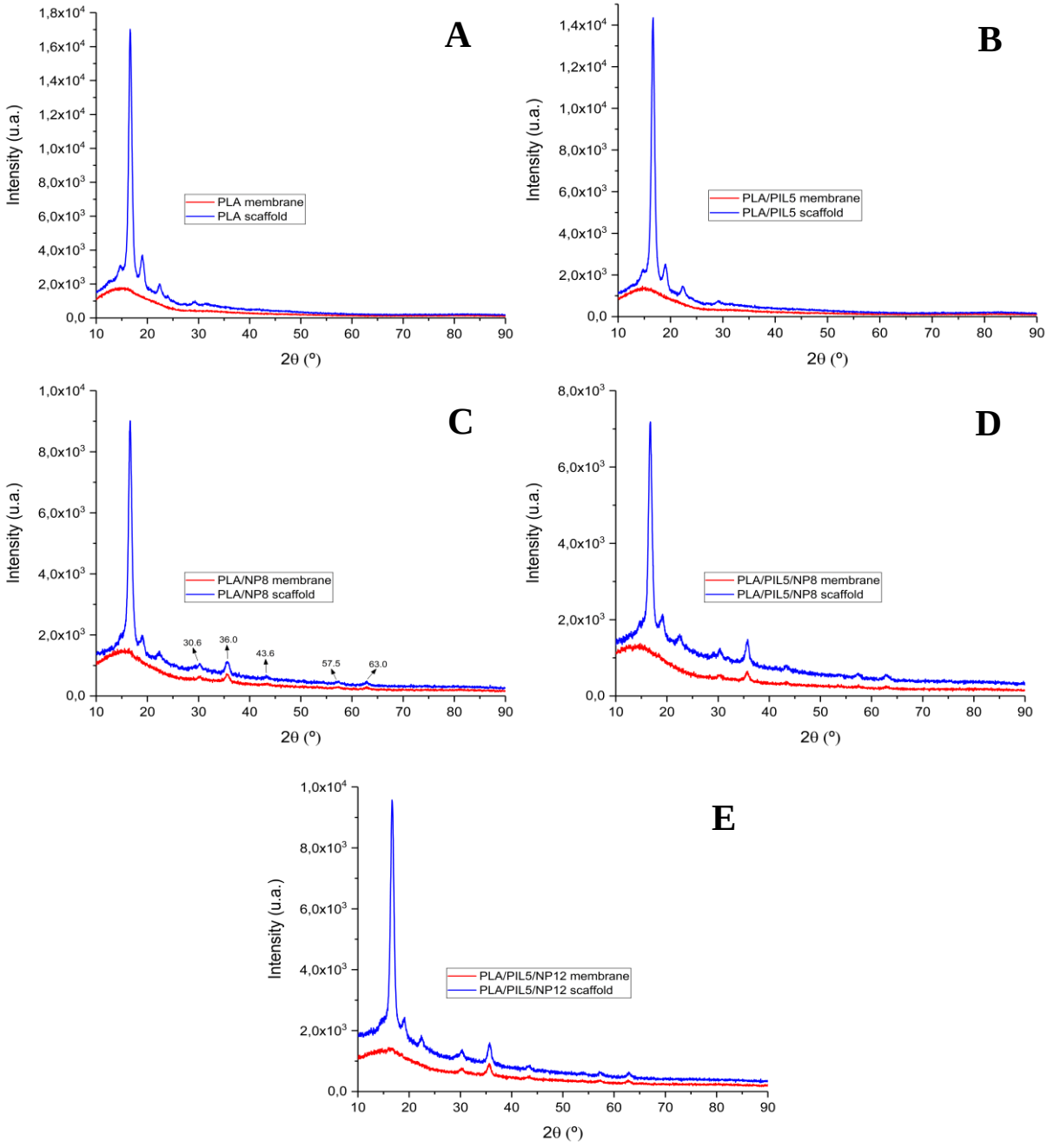

Figure A4 - XRD diffractograms of all the samples comparing the spectrum of the membranes and the scaffolds: A) PLA; B) PLA/PIL5; C) PLA/NP8; D) PLA/PIL5/NP8; E) PLA/PIL5/NP12.